Rapid Communications

Unraveling the nature of universal dynamics in $O(N)$ theories

Kirill Boguslavski[1,2] and Asier Piñeiro Orioli[3,4]

[1]*Institute for Theoretical Physics, Technische Universität Wien, 1040 Vienna, Austria*
[2]*Department of Physics, University of Jyväskylä, P.O. Box 35, 40014 Jyväskylä, Finland*
[3]*JILA, Department of Physics, University of Colorado, Boulder, Colorado 80309, USA*
[4]*Center for Theory of Quantum Matter, University of Colorado, Boulder, Colorado 80309, USA*

(Received 22 November 2019; accepted 4 May 2020; published 15 May 2020)

Many-body quantum systems far from equilibrium can exhibit universal scaling dynamics which defy standard classification schemes. Here, we disentangle the dominant excitations in the universal dynamics of highly occupied N-component scalar systems using unequal-time correlators. While previous equal-time studies have conjectured the infrared properties to be universal for all N, we clearly identify for the first time two fundamentally different phenomena relevant at different N. We find all $N \geq 3$ to be indeed dominated by the same Lorentzian "large-N" peak, whereas $N = 1$ is characterized instead by a non-Lorentzian peak with different properties, and for $N = 2$, we see a mixture of two contributions. Our results represent a crucial step toward obtaining a classification scheme of universality classes far from equilibrium.

DOI: 10.1103/PhysRevD.101.091902

I. INTRODUCTION

Universality constitutes a powerful tool to understand complex many-body systems. A remarkable example is equilibrium phase transitions, where theories can be classified into universality classes based on only few system parameters [1]. Out of equilibrium, while a comprehensive picture is lacking, universal scaling phenomena have been found in turbulence [2], coarsening [3], aging [4], or driven-dissipative systems [5]. In recent years, new far-from-equilibrium universality classes for isolated quantum systems have been theoretically identified [6–24], which have recently started to be probed in cold-atom experiments [25–29]. These universality classes can encompass vastly different theories such as gauge and scalar theories [20,30], or relativistic and nonrelativistic theories [12]. These unexpected connections raise the question of what the relevant physics behind the observed universality is.

The study of these far-from-equilibrium universality classes in isolated systems has so far primarily focused on the properties of *equal-time* momentum distribution functions, $f(t, p)$. These functions describe the occupancy of momentum modes $f \sim \langle \hat{a}_p^\dagger \hat{a}_p \rangle$ for a suitably defined basis of excitations $\hat{a}_p$. The typical scenario is depicted in Fig. 1(a). Starting with high occupation numbers, which may be obtained, e.g., from instabilities or strong cooling quenches [25,26], the system quickly approaches an attractor solution characterized by self-similar scaling, $f(t, p) = t^\alpha f_S(t^\beta p)$, also referred to as nonthermal fixed point. During this phase, the evolution is determined by the universal exponents α, β, and the universal function f_S, which are largely insensitive to system parameters and details of the initial conditions.

Scalar field theories with $O(N)$ symmetry have been shown to exhibit such universal dynamics. In the *infrared*, they are characterized by $\alpha = \beta d$ and $\beta \approx 1/2$ in d spatial dimensions [12]. The physics is linked to particle number transport toward low momenta and the growth of a zero-mode condensate. Remarkably, previous works have found α, β, and the form of f_S to be universal for all values of N [see Fig. 1(b)], including both relativistic $O(N)$ and nonrelativistic $U(N)$ theories describing ultracold Bose gases [12–16]. The origin of this universality has remained so far a mystery. Both exponents and scaling function have been successfully calculated using a large-N kinetic theory, which describes elastic collisions of quasiparticles with free dispersion and a renormalized interaction [12–15,31]. However, it is unclear if and why this description should apply at small N as well. At the same time, descriptions based on defects, e.g., vortices, have provided alternative explanations of related models at small N [10,11,32,33].

In this paper, we resolve this long-standing puzzle on the universality observed in $O(N)$ scalar theories using instead *unequal-time* (two-point) correlation functions. By providing information on both occupancies and dispersion relations, these observables allow us to identify the dominant far-from-equilibrium excitations [34,35], and further provide access to the universal dynamical exponent z [36–42].

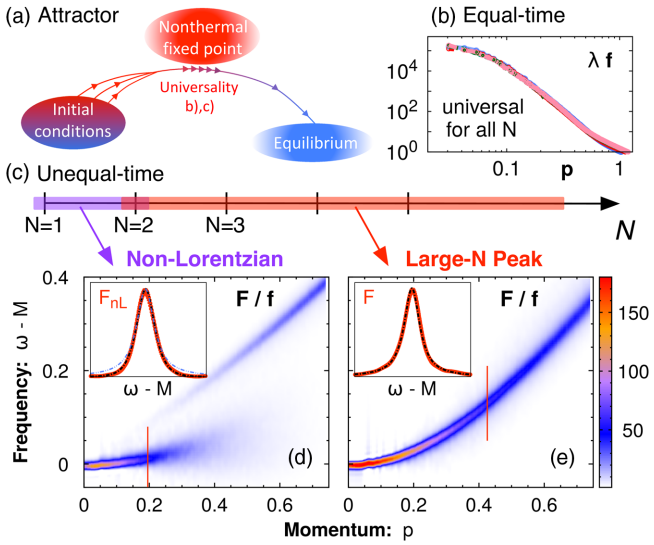

FIG. 1. (a) Typical thermalization scenario for large initial occupancies; the system approaches an attractor during its evolution. (b) The distribution function $f(t,p)$ at low momenta close to the attractor for $N=1$, 2, 3, 4, 8 at times $t=600$, 600, 750, 1000, 2000, respectively. (c) Illustration of universality classes for different N. Statistical function $F(\tau,\omega,p)/f(\tau,p)$ for $N=1$ (d) and $N=8$ (e) at $\tau=1000$. Red lines correspond to F at fixed p, also shown in the insets. Black dashed lines are fits with Eqs. (5) and (3), respectively. $F_{\rm nL}$ is shown after filtering out other small peaks. A (blue dashed) Lorentzian curve is included for comparison.

As our main result, we find that the previously believed N-universality actually breaks up into (at least) two clearly distinct universality classes characterized by different phenomena, which are, however, almost indistinguishable from equal-time correlators and even the dynamical critical exponent z alone.

II. $O(N)$ THEORIES AND STATISTICAL FUNCTION

We consider an $O(N)$-symmetric scalar field theory for relativistic scalar fields $\varphi_a(t,\mathbf{x})$, $a=1,\ldots,N$, in $d=3$ spatial dimensions with classical action ($c=k_{\rm B}=\hbar=1$)

$$S[\varphi]=\int_{t,\mathbf{x}}\left[\frac{1}{2}\partial^\mu\varphi_a\partial_\mu\varphi_a-\frac{m^2}{2}\varphi_a\varphi_a-\frac{\lambda}{4!N}(\varphi_a\varphi_a)^2\right]. \quad (1)$$

Here, $\int_{t,\mathbf{x}}\equiv\int {\rm d}t\int {\rm d}^3x$, and sum over repeated indices is implied. We consider a weak coupling $\lambda\ll 1$ and different values of m. However, since field fluctuations generate an effective mass $M>m$, the exact value of m is not relevant for the infrared physics discussed in this work.

We focus first on the unequal-time *statistical function*, defined for a translation invariant system as the anti-commutator expectation value of scalar Heisenberg field operators $\hat{\varphi}_a$,

$$F(t,t',\mathbf{x}-\mathbf{x}')=\frac{1}{2N}\langle\{\hat{\varphi}_a(t,\mathbf{x}),\hat{\varphi}_a(t',\mathbf{x}')\}\rangle_c, \quad (2)$$

where c denotes the connected part. Introducing the center and relative time coordinates, $\tau\equiv(t+t')/2$ and $\Delta t=t-t'$, we Fourier transform it according to $F(\tau,\omega,\mathbf{p})\equiv\int d\mathbf{x}\int d\Delta t e^{i(\omega\Delta t-\mathbf{px})}F(t,t',\mathbf{x})$.

The statistical function can be seen as an unequal-time generalization of the distribution function, which at low momenta $p\equiv|\mathbf{p}|\lesssim M$ is given by $f(t,\mathbf{p})\approx F(t,t,\mathbf{p})M$ [43]. F contains information not only about the occupancy of excitations in the system but also about their frequency dependence. Thus, the information contained in F can be crucial to understand *which* excitations dominate the dynamics of a system.

We consider far-from-equilibrium initial conditions with large (Gaussian) fluctuations up to a characteristic scale Q as given by $f(t=0,\mathbf{p})=\frac{n_0}{\lambda}\Theta(Q-p)$. Due to the initial "overoccupation" of mode excitations around Q, the subsequent redistribution dynamics is dominated by transport of particles to lower momenta, and is characterized by universal scaling in the infrared as explained in the Introduction.

To describe the system we employ classical-statistical simulations (Truncated Wigner Approximation), which are justified in the limit of high occupancies and small couplings as considered here [44–47]. We perform large-scale simulations averaging over up to 40 runs using $n_0=100$, and give all dimensionful quantities in units of Q. We use either $m=0$ or $m=0.5$ and extract M from our data. F is computed from a classical correlation function, and the relative-time Fourier transforms are performed using standard signal-processing methods. If not stated otherwise, we show data for $\tau=1000$. Further details are given in the Supplementary Material [48].

III. LARGE-N PEAK

We consider first the dynamics in the large-N limit. In general, the statistical function F exhibits several peaks at different frequencies. However, for large N, we find the signal to be clearly dominated by one single contribution, as shown for $N=8$ in Fig. 1(e). We refer to it as the "large-N peak." This peak is depicted for fixed p in the inset (red points), including error bars. It is well described by a Lorentzian parametrized as

$$F_{\rm largeN}(\tau,\omega,p)\simeq\frac{A_{\rm largeN}(\tau,p)\gamma_{\rm largeN}(\tau,p)}{(\omega-\omega_{\rm largeN}(p))^2+\gamma_{\rm largeN}(\tau,p)^2}, \quad (3)$$

which is shown as a black dashed line and accurately agrees with the data.

The results of the fitting procedure with Eq. (3) are shown in the right column of Fig. 2 for $N=8$. The dispersion relation [Fig. 2(b)] is time independent and accurately agrees with a free-particle dispersion of the form

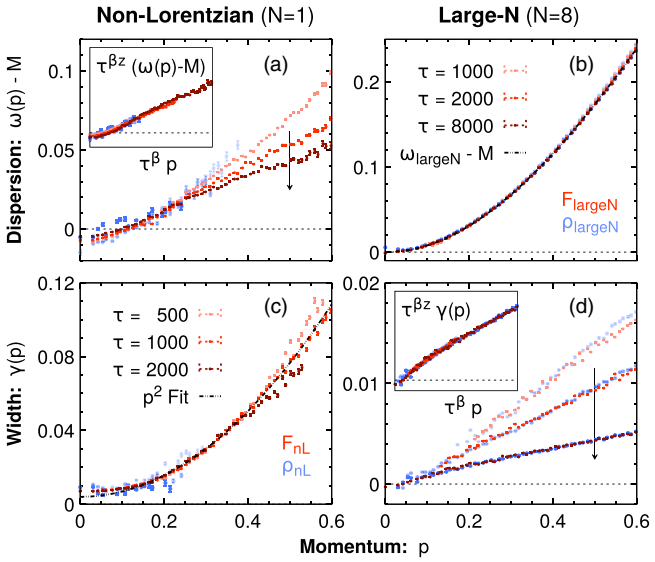

FIG. 2. Dispersion relations $\omega(p) - M$ (a,b) and peak width $\gamma(p)$ (c,d) at different times for the dominating peak of $N = 1$ (a,c) and $N = 8$ (b,d), extracted from F (red) and ρ (blue). Arrows mark their time evolution. Insets show rescaled data ($\beta = 1/2$, $z = 2$).

$\omega_{\text{largeN}}(p) = \sqrt{p^2 + M^2}$. Hence, the dispersion scales quadratically at low momenta as $\omega_{\text{largeN}} - M \sim p^2/(2M)$, implying a dynamical critical exponent $z = 2$.

The decay rate, on the other hand, decreases with time and depends approximately linearly on momentum at low p [Fig. 2(d)]. As shown in the inset, its time evolution obeys self-similar scaling given by $\gamma_{\text{largeN}}(\tau, p) = \tau^{-\beta z}\gamma_{\text{largeN},S}(\tau^\beta p)$ with $\beta = 1/2$ and $z = 2$, consistent with the dispersion. Interestingly, we find that the lifetime of the large-N quasiparticles grows with time since $\gamma_{\text{largeN}}(\tau, p) \to 0$, such that the form of the large-N peak approaches a δ-function.

The dominance of this peak implies $F_{\text{largeN}}(\tau, \omega, p) \approx F(\tau, \omega, p)$ and $A_{\text{largeN}}(\tau, p) \approx f(\tau, p)/M$. Together with the scaling behavior of the dispersion and width, this leads to a self-similar evolution

$$F(\tau, \omega, p) = \tau^{\alpha+\beta z} F_S(\tau^{\beta z}(\omega - M), \tau^\beta p). \tag{4}$$

To understand the nature of the large-N excitations, we study the behavior of fluctuations with the classical equation of motion $[\partial_\mu \partial^\mu + m^2 + \frac{\lambda}{6N}\varphi_b\varphi_b]\varphi_a = 0$ (see Supplemental Material [48] for details). This equation has stable rotating solutions parametrized by $\vec{\varphi}_0(t, \mathbf{x}) = |\vec{\varphi}_0|\mathbf{e}(t)$, where $\ddot{\mathbf{e}}(t) = -M^2\mathbf{e}(t)$. They correspond to rotations in a two-dimensional hyperplane in φ-space, which have been observed numerically [16]. By studying linear fluctuations around these solutions, we find two in-plane (phase and radial) excitations, and a set of $\sim N$ out-of-plane excitations which correspond to rotations perpendicular to the plane spanned by $\mathbf{e}(t)$ and $\dot{\mathbf{e}}(t)$. The out-of-plane excitations have a $\sqrt{p^2 + M^2}$ dispersion and dominate in the large-N limit. These excitations correspond to the large-N peak discussed here.

IV. $N = 1$ NON-LORENTZIAN PEAK

We consider now the statistical function F of a single-component theory as shown in Fig. 1(d). At low momenta $p \lesssim 0.4$, it is again dominated by a single peak [49], shown for fixed p in the inset (red points). While a Lorentzian fit (blue dashed line) with (3) fails to capture the tails of the peak, we find it to be phenomenologically well described by (black dashed curve)

$$F_{\text{nL}}(\tau, \omega, p) \simeq \frac{\pi}{2}\frac{A_{\text{nL}}(\tau, p)}{\gamma_{\text{nL}}(p)}\,\text{sech}\left[\frac{\pi}{2}\frac{\omega - \omega_{\text{nL}}(\tau, p)}{\gamma_{\text{nL}}(p)}\right], \tag{5}$$

where the subscript nL stands for non-Lorentzian.

We employ this form as a fit function to extract the properties of this peak leading to the results in the left column of Fig. 2. The dispersion relation $\omega_{\text{nL}}(\tau, p)$ [Fig. 2(a)] is approximately linear and obeys a self-similar scaling form $\omega_{\text{nL}}(\tau, p) - M = \tau^{-\beta z}\tilde{\omega}_S(\tau^\beta p)$ with exponents $\beta = 1/2$ and $z = 2$, as shown in the inset. The decay rate $\gamma_{\text{nL}}(p)$ [Fig. 2(c)] is found to be instead time independent and to scale as $\gamma_{\text{nL}} \sim p^z$. This implies a self-similar evolution as in Eq. (4), notably with the same scaling exponents as for the large-N peak and $A_{\text{nL}}(\tau, p) \approx f(\tau, p)/M$.

Remarkably, we find the properties of this non-Lorentzian peak to be identical to the infrared peak found in Ref. [35] for a nonrelativistic $U(1)$ complex scalar theory. This can be explained by noticing that at small momenta, $p \ll M$, particle number changing processes are suppressed and the $O(1)$ theory is hence described by an emergent nonrelativistic $U(1)$ theory. The mapping can be made more rigorous by defining the nonrelativistic degrees of freedom $\psi = e^{iMt}[\sqrt{\omega_x}\varphi + i/\sqrt{\omega_x}\pi]/\sqrt{2}$ with $\pi = \dot{\varphi}$ and $\omega_x = \sqrt{M^2 - \nabla^2}$ [33,50].

V. INTERMEDIATE N

Which of these two distinct physical phenomena, if any, dominates for intermediate N at low momenta is *a priori* not obvious.

We find that the $N = 2$ theory is a special case. The statistical function F appears to have two distinct contributions with a similar weight at low momenta, as shown in Fig. 3(a). The inset shows a fit (black dashed line) to these peaks with the sum of both functions (5) and (3). Each of these peaks is included in the inset as separate dashed lines (green and yellow), and their respective dispersions are shown in the main plot. We find that the dispersion of the left peak agrees with ω_{nL} of the non-Lorentzian peak in $O(1)$ theory, while the dispersion of the right peak obeys approximately ω_{largeN} of the large-N peak. However, at low

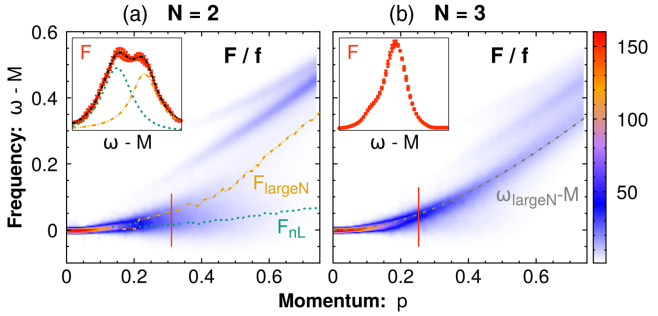

FIG. 3. Statistical function $F(\tau,\omega,p)/f(\tau,p)$ for $N=2$ (a) and $N=3$ (b). The insets show F (red) for the fixed momentum marked by the vertical red lines. (a) green/yellow dashed lines show the peak positions extracted from fits, as well as the fit results in the inset. (b) a relativistic dispersion (gray) is added for comparison.

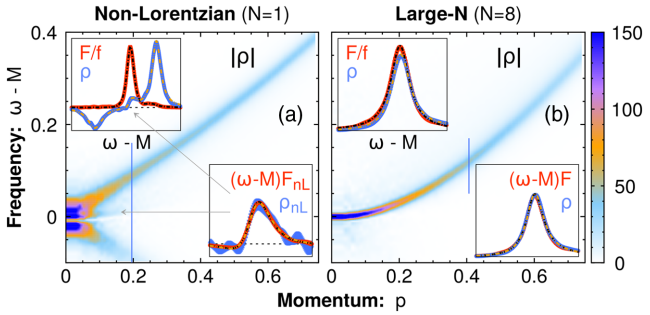

FIG. 4. Spectral function $|\rho|$ for $N=1$ (a) and $N=8$ (b). The upper insets show $F/f(\tau,p)$ and ρ for fixed p marked by vertical blue lines. The lower insets show the validity of Eq. (7) by comparing $(\omega-M)F$ and ρ, both normalized to weight 1. The ratio of normalizations gives $T_{\rm nL}(\tau,p)$. Black/yellow dashed lines are fits to F, ρ.

momenta, both contributions overlap so strongly that they become almost indistinguishable. Therefore, their $p\to 0$ asymptotic behavior is hard to extract.

For $N\geq 3$, we find the infrared dynamics to be dominated by the large-N peak. The statistical function for $N=3$ is shown in Fig. 3(b) and for fixed momentum in the inset. The dominant peak has a dispersion that agrees with $\omega_{\rm largeN}(p)$ (gray dashed line), and we confirmed that the width shows a similar behavior as in the large-N limit. We note, however, that for small N we find evidence of an additional contribution overlapping with the main peak at lower frequencies. Based on the above, this is possibly related to a non-Lorentzian contribution, which appears to quickly disappear as N or momentum increases.

VI. SPECTRAL FUNCTION AND GENERALIZED FDR

To further characterize the non-Lorentzian and large-N Lorentzian peaks, we study the spectral function defined as

$$\rho(t,t',\mathbf{x}-\mathbf{x}')=\frac{i}{N}\langle[\hat{\varphi}_a(t,\mathbf{x}),\hat{\varphi}_a(t',\mathbf{x}')]\rangle. \tag{6}$$

At equal times, $t=t'$, it is determined by the equal-time commutation relations, $\rho|_{t=t'}=0$ and $\partial_t\rho|_{t=t'}=\delta(\mathbf{x}-\mathbf{x}')$. For unequal times, this quantity encapsulates the linear response of the system to perturbations and thus contains information about the low-lying excitations of the system. To compute it, we employ a linear response approach as described in Refs. [34,35] (see Ref. [48] for details).

In Fig. 4, we show color plots of the spectral function for $N=1$ and $N=8$. In general, we find that ρ shows the same peak structure as F but with different relative weights between the peaks. However, since ρ does not contain information about occupancies, the weight of the peaks does not reveal the dominant excitations.

In particular, for $N=1$, we find that the non-Lorentzian peak in ρ has a very small weight [51] [upper inset of Fig. 4(a)], which becomes visible only at low momenta. Nevertheless, this peak has the same dispersion and width as the peak in F [blue points in Figs. 2(a) and (c)]. In fact, we find that the non-Lorentzian peaks in F and ρ fulfill a generalized fluctuation-dissipation relation (FDR) given by

$$F_{\rm nL}(\tau,\omega,p)\simeq\frac{T_{\rm nL}(\tau,p)}{\omega-\mu}\rho_{\rm nL}(\tau,\omega,p). \tag{7}$$

We show this in the lower inset of Fig. 4(a) by filtering out all peaks but the non-Lorentzian peak [48]. Here, $\mu\equiv M$ is an effective chemical potential linked to the approximate conservation of particle number at low momenta. Equation (7) is reminiscent of the equilibrium FDR [52], except with a mode-dependent temperature $T_{\rm nL}(\tau,p)$.

In the large-N limit, the spectral function is dominated by the large-N peak [Fig. 4(b)] with a dispersion and width which also match the results for the corresponding large-N peak in F [Figs. 2(b) and 2(d)]. The two peaks can again be related through a generalized FDR as in Eq. (7) [lower inset of Fig. 4(b)]. However, since the large-N peak dominates in both F and ρ, and since its width becomes narrower with time, Eq. (7) can be simplified in the long-time, large-N limit to

$$F_{\rm largeN}(\tau,\omega,p)\simeq f(\tau,p)\rho_{\rm largeN}(\tau,\omega,p). \tag{8}$$

This is again similar to the thermal case, except with a time-dependent nonequilibrium distribution, and is reminiscent of kinetic approximations [53]. At intermediate $N\geq 3$, we find small deviations from this behavior, which vanish as $N\to\infty$.

VII. DISCUSSION

Our results reveal the existence of (at least) two distinct infrared universality classes governed by two different types of phenomena, despite being characterized by very similar universal exponents.

For $N \geq 3$, the dynamics is dominated by a Lorentzian large-N peak. It results from a set of excitations with relativistic dispersion $\sqrt{p^2 + M^2}$ which dominate due to their number scaling with N. The fact that this physics dominates even at low N is, however, remarkable, especially for $N = 3$ where only one such excitation exists. A possible explanation for this is the fact that the dispersion $\omega_p - M$ scales as $\sim p^2$ in the infrared. Thus, at low momenta, large-N excitations are energetically easier to excite compared to the Bogoliubov mode which scales as $\sim p$ and other excitations with larger effective mass [48]. Apart from this, given that the lifetime of these quasiparticles grows with time, and the fact that they fulfill the generalized FDR of Eq. (8), our results validate the analytic large-N kinetic theory used in Refs. [12–14].

For $N = 1$, the dynamics is instead dominated by a peak of non-Lorentzian shape with time-dependent dispersion and time-independent quadratic width, which coincides with the findings for the nonrelativistic $U(1)$ theory [35]. This hints at a common origin for these infrared excitations. We suggest that this non-Lorentzian peak in $O(1)$ corresponds to vortex line excitations in effective nonrelativistic degrees of freedom. This claim is motivated by previous works on $U(1)$ dynamics [8,10] and $O(1)$ dynamics [16,33], where evidence of vortex excitations was seen in real-space snapshots of the field.

Our results for $N = 2$ show a mixture of two different contributions. We found evidence that one contribution has a $\sqrt{p^2 + M^2}$ dispersion, analogously to the large-N peak. Analytically, however, we do not find any excitation with such a dispersion for the $O(2)$ theory [48]. The second contribution was found to share the same properties as the non-Lorentzian peak of $O(1)$. Thus, we hypothesize that these two peaks possibly originate from vortex-type excitations and domain walls, such as those observed in Refs. [11,16]. In turn, this could explain why the non-Lorentzian contribution is suppressed at large N. Vortex and domain wall excitations can be easily unwound or smoothed out in configuration space when φ_a has $N \geq 3$-components. Thus, they are not stable enough to contribute to the self-similar dynamics at large N.

VIII. CONCLUSION

In this work, we have disentangled the physical origin of the infrared universal dynamics of $O(N)$ scalar theories. Despite equal-time properties being universal for all N, unequal-time correlators have allowed us to identify at least two distinct universality classes as a function of N: non-Lorentzian excitations for $N = 1$ and Lorentzian rotational excitations for $N \geq 3$, while for $N = 2$, we find a mixture. This constitutes a crucial step in classifying universality classes far from equilibrium. In a broader context, our work shows the importance of the unequal-time statistical function F to reveal the dominant physical phenomena in far-from-equilibrium systems, and will potentially trigger future research in this direction. In particular, measuring unequal-time functions [54,55] could substantially improve our understanding of running cold-atom experiments.

ACKNOWLEDGMENTS

We are grateful to J. Berges, T. Gasenzer, T. Lappi, and S. Schlichting for helpful discussions and collaboration on related work. The authors wish to acknowledge CSC—IT Center for Science, Finland, and the Vienna Scientific Cluster (VSC) for computational resources.

[1] N. Goldenfeld, *Lectures On Phase Transitions And The Renormalization Group* (CRC Press, Boca Raton, FL, 2018).
[2] V. Zakharov, V. L'vov, and G. Falkovich, *Kolmogorov Spectra of Turbulence I: Wave Turbulence*, Springer Series in Nonlinear Dynamics (Springer-Verlag, Berlin, Heidelberg, 1992).
[3] A. J. Bray, Adv. Phys. **51**, 481 (2002).
[4] P. Calabrese and A. Gambassi, J. Phys. A **38**, R133 (2005).
[5] L. M. Sieberer, S. D. Huber, E. Altman, and S. Diehl, Phys. Rev. Lett. **110**, 195301 (2013).
[6] J. Berges, A. Rothkopf, and J. Schmidt, Phys. Rev. Lett. **101**, 041603 (2008).
[7] R. Micha and I. I. Tkachev, Phys. Rev. Lett. **90**, 121301 (2003).
[8] B. Nowak, D. Sexty, and T. Gasenzer, Phys. Rev. B **84**, 020506 (2011).
[9] J. Berges and D. Sexty, Phys. Rev. Lett. **108**, 161601 (2012).
[10] B. Nowak, J. Schole, D. Sexty, and T. Gasenzer, Phys. Rev. A **85**, 043627 (2012).
[11] T. Gasenzer, B. Nowak, and D. Sexty, Phys. Lett. B **710**, 500 (2012).
[12] A. Piñeiro Orioli, K. Boguslavski, and J. Berges, Phys. Rev. D **92**, 025041 (2015).
[13] R. Walz, K. Boguslavski, and J. Berges, Phys. Rev. D **97**, 116011 (2018).
[14] I. Chantesana, A. Piñeiro Orioli, and T. Gasenzer, Phys. Rev. A **99**, 043620 (2019).
[15] A. N. Mikheev, C.-M. Schmied, and T. Gasenzer, Phys. Rev. A **99**, 063622 (2019).
[16] G. D. Moore, Phys. Rev. D **93**, 065043 (2016).
[17] J. Berges and B. Wallisch, Phys. Rev. D **95**, 036016 (2017).
[18] J. Berges, K. Boguslavski, and S. Schlichting, Phys. Rev. D **85**, 076005 (2012).

[19] J. Berges, K. Boguslavski, S. Schlichting, and R. Venugopalan, Phys. Rev. D **89**, 074011 (2014).
[20] J. Berges, K. Boguslavski, S. Schlichting, and R. Venugopalan, Phys. Rev. Lett. **114**, 061601 (2015).
[21] K. Boguslavski, A. Kurkela, T. Lappi, and J. Peuron, Phys. Rev. D **100**, 094022 (2019).
[22] S. Bhattacharyya, J. F. Rodriguez-Nieva, and E. Demler, arXiv:1908.00554.
[23] P. E. Dolgirev, M. H. Michael, A. Zong, N. Gedik, and E. Demler, arXiv:1910.02518.
[24] M. Mace, N. Mueller, S. Schlichting, and S. Sharma, arXiv:1910.01654.
[25] M. Prüfer, P. Kunkel, H. Strobel, S. Lannig, D. Linnemann, C.-M. Schmied, J. Berges, T. Gasenzer, and M. K. Oberthaler, Nature (London) **563**, 217 (2018).
[26] S. Erne, R. Bücker, T. Gasenzer, J. Berges, and J. Schmiedmayer, Nature (London) **563**, 225 (2018).
[27] C. Eigen, J. A. P. Glidden, R. Lopes, E. A. Cornell, R. P. Smith, and Z. Hadzibabic, Nature (London) **563**, 221 (2018).
[28] M. Prüfer, T. V. Zache, P. Kunkel, S. Lannig, A. Bonnin, H. Strobel, J. Berges, and M. K. Oberthaler, arXiv:1909.05120.
[29] T. V. Zache, T. Schweigler, S. Erne, J. Schmiedmayer, and J. Berges, Phys. Rev. X **10**, 011020 (2020).
[30] J. Berges, K. Boguslavski, M. Mace, and J. M. Pawlowski, arXiv:1909.06147.
[31] J. Berges and D. Sexty, Phys. Rev. D **83**, 085004 (2011).
[32] M. Karl and T. Gasenzer, New J. Phys. **19**, 093014 (2017).
[33] J. Deng, S. Schlichting, R. Venugopalan, and Q. Wang, Phys. Rev. A **97**, 053606 (2018).
[34] K. Boguslavski, A. Kurkela, T. Lappi, and J. Peuron, Phys. Rev. D **98**, 014006 (2018).
[35] A. Piñeiro Orioli and J. Berges, Phys. Rev. Lett. **122**, 150401 (2019).
[36] A. Schachner, A. Piñeiro Orioli, and J. Berges, Phys. Rev. A **95**, 053605 (2017).
[37] A. Maraga, A. Chiocchetta, A. Mitra, and A. Gambassi, Phys. Rev. E **92**, 042151 (2015).
[38] A. Chiocchetta, A. Gambassi, S. Diehl, and J. Marino, Phys. Rev. Lett. **118**, 135701 (2017).
[39] G. Aarts, Phys. Lett. B **518**, 315 (2001).
[40] S. Sachdev, *Quantum Phase Transitions* (Cambridge University Press, Cambridge, England, 2011).
[41] J. Berges, S. Schlichting, and D. Sexty, Nucl. Phys. **B832**, 228 (2010).
[42] S. Schlichting, D. Smith, and L. von Smekal, Nucl. Phys. **B950**, 114868 (2020).
[43] More generally, it is usually defined as $f(t,p) \equiv [F(t,t,\mathbf{p})\partial_t\partial_{t'}F(t,t',\mathbf{p})|_{t=t'}]^{1/2}$ [53].
[44] G. Aarts and J. Berges, Phys. Rev. Lett. **88**, 041603 (2002).
[45] J. Smit and A. Tranberg, J. High Energy Phys. 12 (2002) 020.
[46] J. Berges, K. Boguslavski, S. Schlichting, and R. Venugopalan, J. High Energy Phys. 05 (2014) 054.
[47] A. Polkovnikov, Ann. Phys. (Amsterdam) **325**, 1790 (2010).
[48] See Supplementary Material at http://link.aps.org/supplemental/10.1103/PhysRevD.101.091902 for details on the technical implementation, data analysis and the analytical derivation of the dispersion relations of $O(N)$ excitations.
[49] At larger momenta, a Bogoliubov-like peak with a linear dispersion at low momenta provides the dominant contribution to F, visible as the upper branch in the plot. We derive its dispersion in Ref. [48] and will discuss this and other excitations in a forthcoming work [56].
[50] M. H. Namjoo, A. H. Guth, and D. I. Kaiser, Phys. Rev. D **98**, 016011 (2018).
[51] This is probably why it was not observed for the $U(1)$ theory in Ref. [35], which had a smaller frequency resolution.
[52] L. Kadanoff, G. Baym, and D. Pines, *Quantum Statistical Mechanics*, Advanced Books Classics Series (Westview Press, 1994).
[53] J. Berges, AIP Conf. Proc. **739**, 3 (2004).
[54] P. Uhrich, S. Castrignano, H. Uys, and M. Kastner, Phys. Rev. A **96**, 022127 (2017).
[55] P. Uhrich, C. Gross, and M. Kastner, Quantum Sci. Tech. **4**, 024005 (2019).
[56] K. Boguslavski and A. Piñeiro Orioli (in preparation).